# The mixed layer depth below the pycnocline (BMLD) as an ecological indicator of subsurface chlorophyll-a

Arianna Zampollo[1,*], Thomas Cornulier[1], Rory O'Hara Murray[2], Jacqueline Fiona Tweddle[1], James Dunning[1], Beth E. Scott[1]

[1] School of Biological Sciences, University of Aberdeen, Aberdeen, AB24 2TZ, UK

[2] Marine Scotland Science, Aberdeen, AB11 9DB, UK

*Correspondence to*: Arianna Zampollo (zampolloarianna@gmail.com)

**Abstract**

Primary production dynamics are strongly associated with vertical density profiles in shelf waters. Climate change and artificial structures (e.g. windfarms) are likely to modify the vertical structure of stratification and nutrient fluxes in shelf seas, and hence the vertical distribution and production levels of phytoplankton. To understand the effect of physical changes on primary production, identifying the linkage between water column density and chlorophyll-a (Chl-a) profiles is essential. Here, the biological relevance of eight density levels (DLs) characterizing three different portions of the pycnocline (the top, central aspects, and the bottom) was evaluated to find the best indicator of the vertical distribution of Chl-a in stratified conditions. The association of any DLs with the depth of Chl-a maximum (DCM) was tested using Spearman correlation, linear regression, and a Major Axis analysis with data covering summertime over 15 years in a shelf-sea region (the northern North Sea) that exhibits stratified water columns. Out of 1237 observations of the water column densities exhibiting a pycnocline, 78% reported DCM above the mixed layer depth below the pycnocline (BMLD) with an average distance equal to 2.74 ± 5.21 m. BMLD acts as a vertical boundary at which subsurface Chl-a maxima (SCM) is most frequently found in shelf sea seas (depth ≤ 115 m). Overall, BMLD and indicators of the halfway pycnocline highly predicted the location of DCMs than MLD indicators and maximum squared buoyancy frequency (Max $N^2$). These results confirm a significant contribution of deep mixing processes in subsurface production in stratified waters and indicate BMLD as a valuable tool for understanding the spatiotemporal variability of Chl-a in shelf seas. An analytical approach as a valuable tool to extrapolate BMLD and MLD from *in situ* vertical samples is also proposed.

**Keywords**

deep mixing, depth of Chl-a maxima (DCM), offshore renewables, primary production, subsurface Chl-a maxima (SCM)

## 1. Introduction

As we begin to manage our oceans and shelf seas for more complex simultaneous uses, such as renewable energy developments, fishing and marine protected areas, it is becoming increasingly important to understand the details of primary productivity at fine spatial scales. Besides very shallow waters, the vast majority of phytoplankton production in continental shelf waters generally occurs under stratified conditions, where the pycnocline provides a stable habitat for phytoplankton growth in the lower euphotic zone. The balance between stratification and mixing in the water column is the main determinant for phytoplankton production and in the North Sea, the balance between mixing and stratification has been shown to fluctuate in time and space by the modulation of daily, biweekly and seasonally strong tidal cycles (Klymak et al., 2008; Sharples et al., 2006; Zhao et al., 2019b; Müller et al., 2014), which represent the main source of new nutrients' supply to the pycnocline in prolonged stratified conditions. Turbulent mixing of the water column requires energy sources from either the surface (e.g. wind stress, Ekman pump due to wind curl) or deep waters (e.g. upwelling, eddy diffusion, tidal currents), which can be altered by climate change (Holt et al., 2016, 2018) and the introduction of numerous man-made infrastructures (Dorrell et al., 2022). Therefore, effects are expected in the overall mixing budget of our seas due to both these changes. Anomalies as circulation slow-down, sea-level rise, bottom and surface temperature, wind speed and wave height have largely been described as a consequence of climate change in the last two decades (e.g. Orihuela-Pinto et al., 2022; Taboada and Anadón, 2012; Bonaduce et al., 2019), while the consequences of these changes on the biological processes are still partially understood (Lozier et al., 2011; Somavilla et al., 2017).

### 1.1 Subsurface chlorophyll-a maxima (SCM)

Many of the uncertainties regarding the impacts on primary production come from the difficulties in correctly sampling its abundance in the whole water column. Contrary to the detection of surface blooms by satellite sensors, subsurface chlorophyll-a maxima (SCM) are often more difficult to measure. SCM represents significant features in plankton systems (Cullen, 2015), they define where most of the bottom-up processes take place and can exist in separate vertical layers and encompass more than 50% of the entire water column production (Weston et al., 2005; Takahashi and Hori, 1984). In the North Sea, the summertime (May-August) subsurface production contributes to the annual production of up to 20-50% and sustains the food chain in continental shelf waters during prolonged stratified conditions (Hickman et al., 2012; Richardson and Pedersen, 1998; Weston et al., 2005). Several studies linked the vertical distribution of maximum chlorophyll-a (Chl-a) to deep mixing processes (e.g. Brown et al., 2015; Richardson and Pedersen, 1998; Sharples et al., 2006) and identified the occurrence of deep Chl-a assemblages in the proximity of the pycnocline in shelf seas (e.g. Costa et al., 2020; Durán-Campos et al., 2019; Ross and Sharples, 2007; Sharples et al., 2001). Maxima Chl-a have been identified at the base of the pycnocline in regions of strong tidal mixing at Georges Bank in August (Holligan et al., 1984) and within the western English Channel (Sharples et al., 2001). However, despite the clear linkage between SCM and deep physical processes in shelf seas, surface mixing processes have been used to investigate the global variations of primary production (Somavilla et al., 2017; Steinacher et al., 2010) making the surface mixed layer depth (MLD) an indicator of variations of Chl-a. The use of MLD is motivated in oceanic sites where the deepest limit of the pycnocline is difficult to draw, while the limits of the pycnocline in shelf waters are more evident due to surface and deep mixings confining the pycnocline in a restricted zone.

### 1.2 Mixed layer depth (MLD) and pycnocline characteristics

MLD has been largely considered as a central variable for understanding phytoplankton dynamics (Sverdrup, 1953), especially in oceanic sites, where several studies have investigated the ecological relevance of MLD on Chl-a vertical

distribution (Behrenfeld, 2010; Carranza et al., 2018; Diehl, 2002; Diehl et al., 2002; Gradone et al., 2020), phytoplankton bloom events (Behrenfeld, 2010; Chiswell, 2011; D'Ortenzio et al., 2014; Prend et al., 2019; Ryan-Keogh and Thomalla, 2020, Sverdrup, 1953), and the effects of climate change (Somavilla et al., 2017). The nutricline's depth exhibits positive correlations with the upper mixed layer depth (Ducklow et al., 2007; Gradone et al., 2020; Holligan et al., 1984; Prézelin et al., 2000, 2004; Ryan-Keogh and Thomalla, 2020; Yentsch, 1974, 1980), and it has been generally associated with surface spring blooms or windstorm events (Carranza et al., 2018; Carvalho et al., 2017). However, the effects of MLD and climate's variations on primary production are still an unsolved question (Lozier et al., 2011; Somavilla et al., 2017). The need for a much more detailed understanding of the linkage between primary production, pycnocline characteristics and deep turbulent processes (below the pycnocline) is therefore a key area of research, especially in highly productive but spatially heterogeneous areas such as shelf waters and shallow seas.

The methods for identifying MLDs vary among marine environments, hydrodynamic regimes, or the spatial resolution of vertical profiles (Courtois et al., 2017; Lorbacher et al., 2006), because making use of a single method is difficult for spatiotemporally heterogeneous regions. MLDs are typically defined as the depth at which the density exceeds a specific value (threshold) (e.g. Kara et al., 2000), however this method presents issues in specific hydrodynamic conditions, such as over estimating MLD in regions with deep convection (e.g. subpolar oceans) (Courtois et al., 2017), or misidentifying water columns with a newly established shallow MLD over previous periods of stratification (Somavilla et al., 2017). Several sensitivity tests and comparisons have been conducted in oceanic waters (González-Pola et al., 2007; Holte and Talley, 2009; Courtois et al., 2017), however, there are no standard methods for MLD identification neither in shelf nor oceanic waters.

### 1.3 A new way forward: the mixed layer depth below the pycnocline (BMLD) as a proxy for Chl-a maximum in shelf waters

In this study, we proposed the adaptation of existing methods into a new algorithm able to cope with different high-resolution (1 m) vertical distributions of density (characterized by split pycnoclines and unusual shapes) to identify i) the surface mixed layer (commonly known as MLD) and ii) the mixed layer depth below the pycnocline (BMLD) intended as the depth at which the pycnocline ends and deep mixing develops down to the seabed. The method is validated using vertical samples of density and Chl-a to characterize the relationship between stratification features and subsurface Chl-a in waters depths from 20 to 120 m, with 15 years of repeated surveys that covers a mosaic of habitats types: seasonal stratified waters, permanently mixed waters, regions of freshwater inputs and strong tidal mixing (Leeuwen et al., 2015). The relationships between the vertical distribution of eight different density levels (DL) and Chl-a profiles are analysed using three different analytical techniques for comparisons: Spearman's rank correlation coefficient ($\rho_S$), a Major Axis (MA) line fitting and a linear regression model (LM). This approach is being developed in order to help the identification of key linkages between the physical environment and primary production at finer spatial scales ($\leq$ 1 km), which can be ecologically relevant for pressing issues in marine spatial management (e.g. seabed leasing for wind farms, locations of MPAs) and spatially explicit climate change assessments.

## 2. Methods

### 2.1 Physical and biological oceanographic samples

*In situ* summertime measurements of temperature, salinity, and Chl-a were collected from a towed, undulating, CTD and a vertical CTD in the North Sea off the East coast of Scotland, UK, within the Firth of Forth (FoF) and Tay region for over 15 years (from 2000 to 2014) (Fig. 1). A total of 1273 profiles from both types of sampling were extracted from

April to August (April=3, May=51, June=1115, July=66, August=38). 426 profiles were gathered using the vertical CTD from 12 oceanographic campaigns carried out by Marine Scotland Science on board of the fisheries research vessels *Scotia* and *Alba na Mara* (www.gov.scot/marine-and-fisheries). The data set comprises temperature, conductivity, and Chl-a measurements from the sea surface to the seabed (vertical resolution equals to 1 decibar) at fixed stations sites. Water samples were collected during each cast for calibration of the *in situ* sensor data. The undulating CTD sampled the water column in June 2003 and July 2014 with a continuous vertical and horizontal oscillation of the instrument throughout the water column from 2-5 m below the sea surface to 5 m from the seabed. The continuous profiles obtained from undulating CTD were converted into 847 single profiles of the water columns. Data were sampled at 1 second intervals, resulting in a vertical resolution comprising between 0.5 and 1 m, in water depths from 25 m to 115 m. Further information about the oceanographic cruise in June 2003 is described by Scott et al. (2010), whose method was applied in the cruise in July 2014.

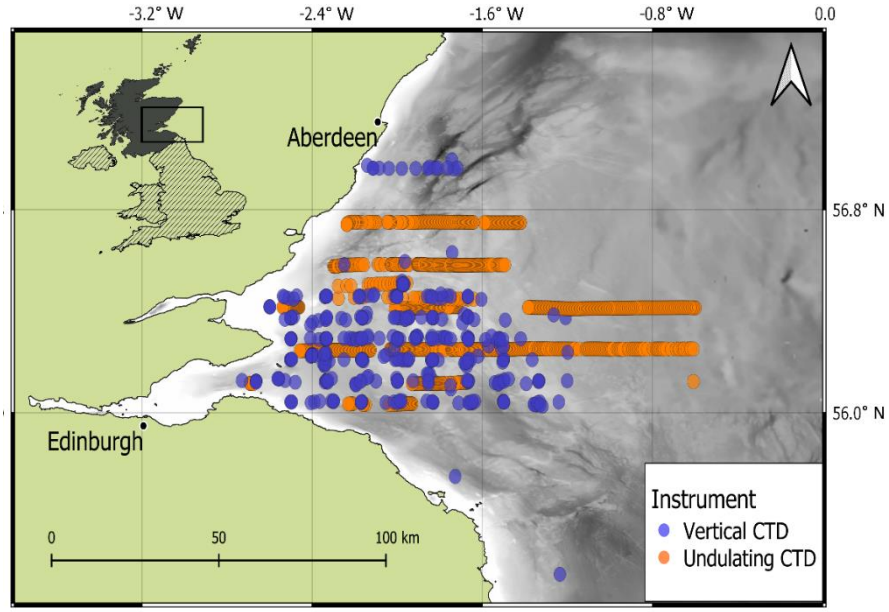


*Figure 1: Study area with the in situ surveys measured by a vertical CTD (blue dots) and an undulating CTD (orange dots). Land (green) and bathymetry (grey colour ramp) are pictured (ESRI 2020; EMODnet 2018)*

### 2.1.1 Standardized density profiles

Since the proposed algorithm (described in Sect. 2.2) works with profiles at high vertical resolution (samples' vertical resolution is 1 m), the *in situ* casts must be standardized throughout the water column. Density ($\rho$) observations taken every 0.5 to 1 m from undulating CTD were converted into measurements over regular depth intervals by smoothing and interpolating. This was achieved by fitting a generalized additive model (GAM) (Hastie and Tibshirani, 1990) using an adaptive spline with $\rho$ as a function of depth. The obtained smooth function for each profile was used to interpolate $\rho$ at regular 1 m depth intervals. In order to maintain the same shape and values in each profile, the fitted curves at 1 m intervals were visually checked by plotting the estimated and real profiles to identify possible errors visually. 4.16% of the shapes ($n$=53) were manually corrected by changing the number of knots in the GAM, which ranged from 75% to 90% of the number of observations occurring within each profile. An example is given in Figure A2 in Appendix A. The analyses were run in R v3.6.3 (R Core Team, 2018) using the *mgcv* v1.8-33 package.

## 2.2 MLD and BMLD detection

*Definition of MLD and BMLD*

In stratified waters, the layers above and below the pycnocline are mixed vertical region where the density gradient is significantly different from the pycnocline. The upper mixed layer depth (MLD) and the mixed layer depth below the pycnocline (BMLD) are both the transition regions between mixed waters and the pycnocline (Fig. 2). The most common threshold methods (see Sect 2.3) identify MLD based on the principle that the mixed layer at the surface has a density's variance close to zero, which separates from the pycnocline, exhibiting a larger density gradient. The above assumptions may not always hold, especially when the upper mixed layer is heterogeneous with nested sub-structures such as small re-stratification at the surface, or when the pycnocline can include a small mixed layer (Fig. A1a, e, f in Appendix A) or presents different density gradients (stratified layers) within it (Fig. A1b and c in Appendix A). Such density conditions are difficult to isolate with the available methods.

In the proposed algorithm, the detection of MLD does not assume that the upper mixed layer has a density gradient close to zero up to the top of the pycnocline, and it identifies MLD (and BMLD) regardless any *a priori* threshold (Chu and Fan, 2019, 2011; Holte and Talley, 2009). Two approaches, the angle's method from Chu and Fan (2011) and K-mean statistics, are used to analyse the vertical distribution of density ($\rho$) by comparing the observations to each other in the same profile instead of applying an absolute threshold to all profiles. The algorithm distinguishes in the water column three layers having similar density values (the upper mixed layer, pycnocline and lower mixed layer) (Fig. 2) using K-mean statistics. The MLD represents the shallowest depth up to which the difference of density between adjacent points $\Delta\rho$ is small and similar from the surface. The BMLD is the first depth below the pycnocline from which $\Delta\rho$ is small and similar down to the seabed. This type of detection based on the density shape allows the identification for unconventional density vertical distribution (Fig. A1 in Appendix A).

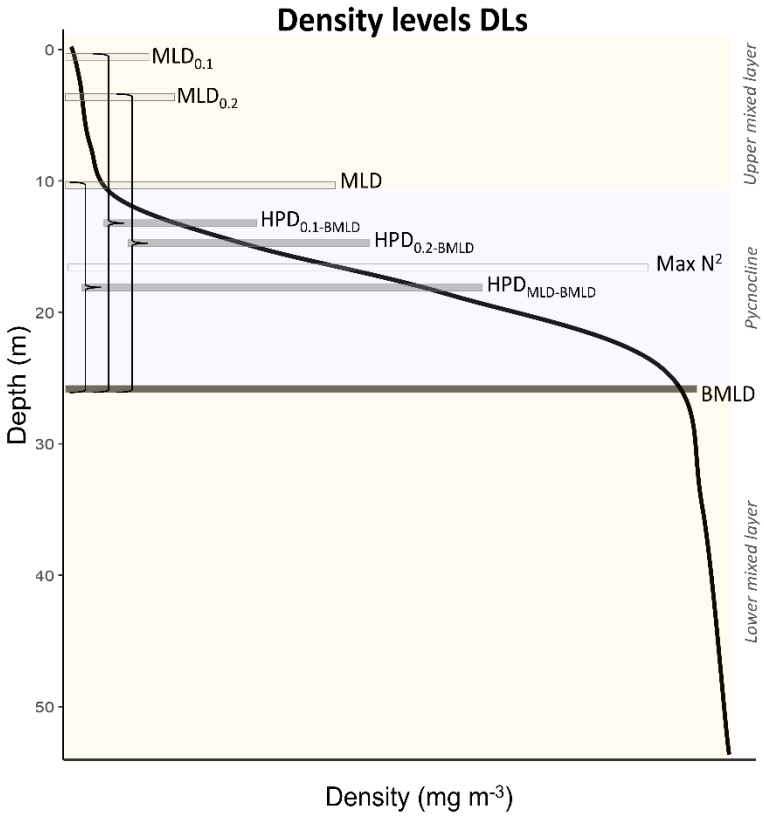

*Figure 2: The eight density levels (DLs) are reported for a generic density profile whose upper mixed layer, pycnocline and lower mixed layer are displayed with different coloured rectangles. The curly brackets define the halfway depths (HPDs) between MLD's indicators ($MLD_{0.1}$, $MLD_{0.2}$, MLD) and BMLD.*

*Method to extract MLD and BMLD*

MLD and BMLD were identified by developing an algorithm in R v3.6.3 (R Core Team, 2018) named *abmld.R*, and available at https://github.com/azampollo/BMLD, that analyses the shape of the density profile and distinguishes a mixed from a stratified layer using i) an adaptation of the maximum angle method (Chu and Fan, 2011) and ii) a cluster analysis on the density difference between two consecutive points ($\Delta\rho_z = |\rho_z - \rho_{z+1}|$). The method is designed to work with equal, high-resolution (1 meter), intervals of density values (z) collected in stratified shelf waters, with a pycnocline detailed by > 5 values, and BMLD distributed within the first 90% of the observations from the surface to the deepest point (close to the seabed). The reason why the method is sensitive to the number of points within the pycnocline, before MLD and after BMLD, is due to the analyses included in the algorithm depending on at least two observations at the beginning of each mixed layer.

The first steps of the algorithm follow the method by Chu and Fan (2011) where the depth exhibiting the maximum angle between two vectors, referring to density conditions above and below it, is selected as the mixed layer depth. At each observation (z) of the density profile, the method calculates the angle (φ) from the intersection of two vectors, V1 and V2, each one fitted using a linear regression model that accounts for the vertical distribution of the density values above (for V1) or below (for V2) *z*. At each *z* of the density profile, a unique V1 (blue line in Fig. 3) is fitted using *z* and 2 points (2δ) above it, and a unique V2 (red line in Fig. 3) is fitted using *z* and 2 points below it. The angle (φ) resulting from the intersection of the two lines is measured in degrees using Eg. 1 reported in Supplementary material. A value of φ is hence associated with each point of the density profile. Although Chu and Fan (2011) suggested to identify MLD by measuring the tangent of the angle between V1 and V2, we encountered some issues identifying BMLD in those profiles where φ was bigger than 90 degrees, and where density slightly decreased below the pycnocline (Fig. A1d, Appendix A). At this point, an angle φ is associated with each observation in the density profile. Since the identifications of MLD and BMLD are both based on the ranking of φ, the selection of either one or the other requires splitting the density profile into "surface" (Split1) and "deep" (Split2) observations to avoid any misidentification and interchange between mixed layer depths. *Split1* includes the density values from the surface ($z_1$) to two measurement intervals (2δ) above BMLD (Fig. 3a), while *Split2* extends from 2δ above the halfway depth in $\rho$ range ($0.5\Delta\rho = ((\rho_{max} - \rho_{min})/2) - 2$) to the ninetieth portion of the profile from the surface to the seabed ($z_{0.9\Delta\rho}$ = 90% of $^{n}_{1}z$) (Fig. 3b). The bottom limit of Split2 was defined at $z_{0.9\Delta\rho}$ following Chu and Fan (2011) to reduce the number of observations close to the seabed. However, the analyses can be extended up to the end of the profile by following the instructions reported at https://github.com/azampollo/BMLD.

After the selection of the largest angles as potential MLD and BMLD, a further K-Mean cluster analysis (Lloyd, 1982) was used to identify the mixed and stratified layers based on the density difference between two consecutive points ($\Delta\rho_z$). The cluster analysis satisfied the assumption that similar observations belong to either the mixed or stratified layers. MLD and BMLD were hence selected above the candidates whether the observations above and below them belonged to the same cluster. More details regarding the decisional tree of the algorithm are reported in the Supplementary materials. Adding the conditions controlling for a similar classification of observations at depths above MLD and below BMLD decisively improved the selection of pycnocline's limits in pycnocline fractured in chunks. Moreover, several trials

reported that the exclusive use of the maximum angle method would have biased the selection due to local variation and instability conditions of the water column (Fig. A1b, c, e, f in Appendix A).

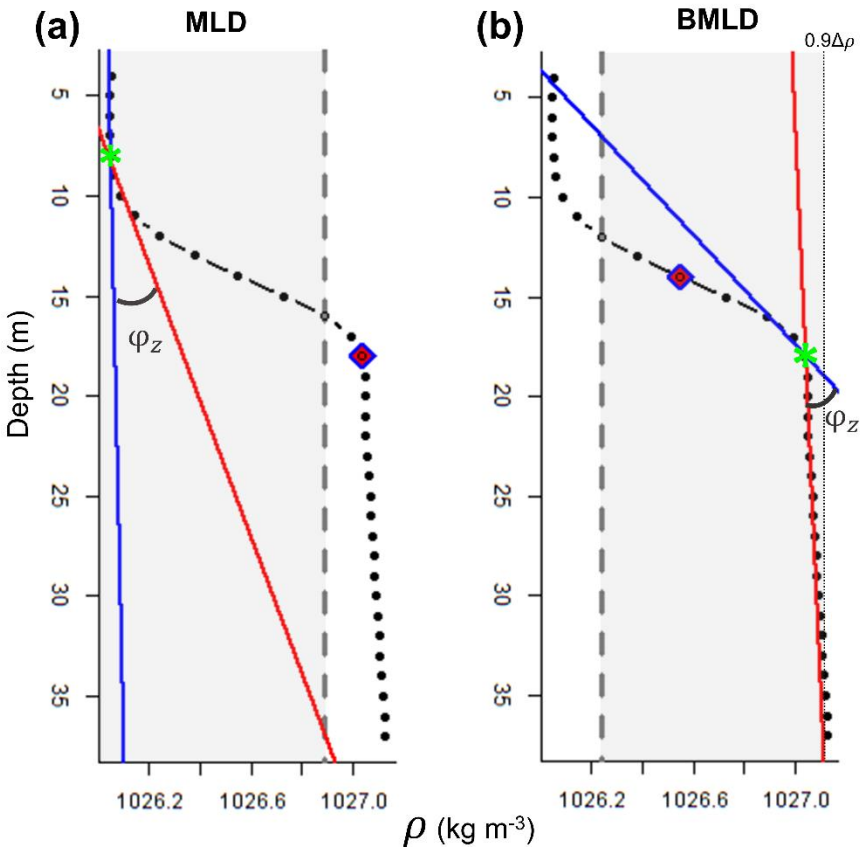


*Figure 3: plots of a density profile reporting the attributes calculated by the algorithm: grey region includes the observations (z) (black dots) used to identify MLD and BMLD, which extends in (a) from the surface to 2δ above BMLD (purple rhombus), and in (b) from 2δ above half of the density range reported by the profile (0.5Δρ, purple rhombus) to 0.9Δρ. The solid blue and red lines refer to the vectors V1 and V2, whose intersection defines the angle $\varphi_z$ selected as MLD and BMLD (green stars).*

*Performance of the algorithm*

The algorithm was validated by manually checking the estimated MLD and BMLD in each profile, which were considered wrongly identified when falling into the pycnocline. Since most of the errors located the mixed layer depths clearly at the centre of the pycnocline having thin layers of re-stratification (> 4 observations) (Fig. A1 b, c, e, f, Appendix A), the identifications were considered correct when they appeared i) on top of a lower mixed layer (in BMLD) and ii) on top of a large density gradient (pycnocline) separating surface to deep waters (in MLD). Major errors in identifying MLD (6.76% of the profiles) and BMLD (4.32%) occurred in density profiles with a smooth transition from the mixed layer to the pycnocline, hence reporting a high number of observations at the mixed layer depths (e.g. Fig. A1 a-c, Appendix A). It is important to highlight the sensitivity of this method to the difference in density ($\Delta\rho$) at MLD and BMLD (a large $\Delta\rho$ is preferred), and to the sampling frequency at the transition regions between mixed waters and the pycnocline. The algorithm did not correctly identify MLD in profiles without an upper mixed layer and a shallow pycnocline that comprised two different gradients (Fig. A1c, Appendix A). In this case, the cluster analysis split $\Delta\rho$ into two groups,

although they belong to the same pycnocline. Other errors were related to profiles having a pycnocline split into two parts by a thin mixed layer having > 4 observations (Fig. A1e, Appendix A). Overall, the identification of BMLD performed better than MLD's, although it could not deal with profiles having less than 4 observations throughout the pycnocline (thickness of the pycnocline < 3 m). This condition occurred due to the location of the *Split2* (which is necessary to distinguish BMLD's from MLD's selection) i) at depths above MLD (misidentifying MLD as BMLD) or ii) too close to BMLD (missing enough observations to fit V1 properly). The algorithm always correctly selected BMLD in profiles with a temporary overturn in the density profile (Fig. A1d, Appendix A).

### 2.3 Common methods identifying Density Levels (DLs)

The depths detailing the density structure in the water column are defined here as density levels (DLs). Among the multiple indicators of mixed layers that associate with Chl-a vertical distribution, the ecological relevance of the MLD, the halfway pycnocline depth and the maximum buoyance depth were compared to the proposed algorithm's identifications.

The MLD is typically defined in the literature as the depth at which the density exceeds a specific value (threshold method) (e.g. Kara et al., 2000). The threshold is typically selected among a range of values previously tested in the literature (from 0.0025 to 0.125 kg $m^{-3}$) (summarized in Thomson and Fine, 2003; Montégut et al., 2004; Lorbacher et al., 2006; Holte and Talley, 2009) and measured as the difference ($\Delta\rho_z = |\rho_z - \rho_{ref}|$) between a certain sampling depth ($z$) and a reference density value ($\rho_{ref}$), which can be the density at the surface, at 10 m depth, or a consecutive point (e.g. $z$-1). In this study, two density thresholds (0.01 and 0.02 kg $m^{-3}$) have been measured as the difference between two consecutive points in the profile ($\Delta\rho_z = |\rho_z - \rho_{z+1}|$) and named as $MLD_{0.01}$ and $MLD_{0.02}$.

Since previous studies identified subsurface Chl-a in the proximity of the centre of the pycnocline (hereafter called halfway pycnocline depth, HPD, Table 1), we investigated the relationship between DCM (depth of maximum Chl-a) and three different HPDs measured as the halfway depth between the base of the pycnocline (BMLD) and $MLD_{0.01}$, $MLD_{0.02}$ and MLD from the proposed algorithm. These DLs are named $HPD_{0.01\text{-}BMLD}$, $HPD_{0.02\text{-}BMLD}$, and $HPD_{MLD\text{-}BMLD}$ (Fig. 2).

Moreover, several studies reported positive correlation between the maximum squared buoyancy frequency (Max $N^2$) and DCM at oceanic sites (e.g. Martin et al., 2010; Schofield et al., 2015; Carvalho et al., 2017; Courtois et al., 2017; Baetge et al., 2020) and shelf waters (Lips et al., 2010; Zhang et al., 2016). Therefore, the depth of Max $N^2$ has been selected from $N^2$ profiles computed by *gsw_Nsquared* function (*gsw* v1.0-5 package) in R v3.6.3 (R Core Team, 2018), following the most recent version of the Gibbs equation of state for seawater in TEOS-10 systems (Intergovernmental Oceanographic Commission, 2010). The magnitude of $N^2$ quantifies the stability of the water column and pinpoints the stratified layers where the energy required to exchange water parcels in the vertical direction is maximum (Boehrer and Schultze, 2009).

*Table 1: Table of abbreviations used in the paper.*

| **Abbreviation** | **Description** |
|---|---|
| *SCM* | *Subsurface Chlorophyll-a maximum* |
| *Chl-a* | *Chlorophyll-a (mg $m^{-3}$)* |
| *DCM* | *Depth of maximum Chlorophyll-a (m)* |
| *DL* | General abbreviation for a *density layer* (e.g. MLD, BMLD, HPD, or Max $N^2$) *(m)* |
| *MLD* | *Mixed layer depth*, or top of the pycnocline *(m)* |
| *BMLD* | *Mixed layer depth below the pycnocline*, or base of the pycnocline *(m)* |

| | |
|---|---|
| *HPD* | *Halfway pycnocline depth*, or centre of the pycnocline *(m)* |
| *Max $N^2$* | maximum squared buoyancy frequency ($N^2$) *(m)* |

### 2.4 Subsurface Chlorophyll-a parameters

The depth of maximum Chl-a (DCM) was defined as the deepest maximum inflection point in the Chl-a profile with 1 m sampling frequency (Carvalho et al., 2017; Zhao et al., 2019b). Here, the inflection point is defined as the depth exhibiting a high concentration of Chl-a and a large change in Chl-a values throughout the profile. The variation of Chl-a throughout the water column was investigated using the adapted Chu and Fan (2011) method identifying for φ that is described in Sect 2.2. The angle (φ) were measured at each depth of the Chl-a profile, and the maximum φ with the largest Chl-a concentration was selected as DCM. The automated identification of DCM was checked manually with a visual inspection of each profile. The portion of the method used to measure the angle φ was integrated into a new function *maxChla.R* coded in R v3.6.3 (R Core Team, 2018) and available at https://github.com/azampollo/BMLD.

The total amount of Chl-a were measured using trapezoidal integration (Walsby, 1997) throughout the water column (depth-integrated Chl-a).

### 2.5 Evaluating the association of density levels with subsurface Chl-a

The ecological relevance of each density level (DL) was evaluated by comparing their coincidence with the depth of maximum Chl-a (DCM) (e.g. DCM = BMLD) and their strength in predicting DCM. The coincidence and the prediction of DCMs from density profiles return important understanding of the processes driving subsurface concentrations and identify a valuable proxy for modelling analyses and for controlling uncertainty in net primary production estimates.

In this study, we evaluated the coincidence of the DCM with eight investigated density levels ($MLD_{0.01}$, $MLD_{0.02}$, MLD, BMLD, $HPD_{0.01\text{-}BMLD}$, $HPD_{0.02\text{-}BMLD}$, $HPD_{MLD\text{-}BMLD}$, and Max $N^2$, Fig. 2) using Spearman's rank correlation coefficient ($\rho_S$) and a Major Axis (MA) line fitting, and the prediction of DCM from DL by performing a linear regression model (LM). All three methods differently assess the level of correlation or prediction. The Spearman's coefficient (Eq. (1) in Table 2) assesses a monotonic linear relationship with values ranging between -1 and +1, which refer to a perfect negative or positive correlation between two variables. Besides the strength of the linear relationship defined by $\rho_S$, we focused on evaluating the linear relationship between DCM and each DL using 3 different linear models $y = \alpha + \beta x$: 1) alpha and beta estimated by linear regression; 2) alpha and beta estimated by major axis line fitting; and 3) the one-to-one linear regression with alpha and beta fixed at 0 and 1 respectively. The one-to-one line hypothesizes that DCM and DL occur at the same depth. The MA is largely used to investigate how one variable scales against another by accounting for errors from both directions ($x$ and $y$) and measuring the residuals perpendicular to the line (details in the review Warton et al., 2006). Therefore, the aim of MA is not to predict the $y$-variable, however evaluating the proximity of the coefficients of the estimated MA line ($\alpha$ and $\beta$) to the scenario in which DL equals DCM. The coincidence of each DL and DCM was summarized by reporting the $\alpha$ and $\beta$ MA coefficients, which are hypothesized to be intercept $\sim 0$ and slope $\sim 1$ when DCM occurs at the same depth of the DL in question.

Since the identification of a proxy for subsurface Chl-a represents a useful tool for correctly assessing the abundance and the variations of primary production, we investigated the power of prediction of DCM from each DL by measuring the r-squared ($R^2$) from i) an ordinary least square to estimate parameters from the observations in a linear regression (Eq. (2) in Table 2), and ii) the one-to-one linear regression (which has been forced with the intercept through the origin and a

slope equal to 1, Eq. (3) in Table 2). The formulae used to calculate the coefficient of determination $R^2$ for the one-to-one ($R_0^2$) and empirical ($R_{em}^2$) LMs are summarized in Eq. (2) and Eq. (3) in Table 2.

*Table 2: Formulae for estimating the bivariate line-fitting. Spearman's rank correlation coefficient ($\rho_S$), coefficient of determination $R^2$ for testing the one-to-one linear regression ($R_0^2$) (e.g. DCM ~ BMLD) and the empirical linear regression ($R_{em}^2$).*

| | Formula | Purpose |
|---|---|---|
| $\rho_S$ | $\frac{\sigma_{xy}}{\sigma_x \sigma_y}$ (1) | Estimate the strength of the relationship between $x$ and $y$ |
| $R_{em}^2$ | $1 - \frac{SS_{RES}}{SS_{TOT}} = 1 - \frac{\sum_{i=1}^{n}(y_i - \hat{y}_i)^2}{\sum_{i=1}^{n}(y_i - \bar{y})^2}$ (2) | Measure the variation in $y$ that is explained by $x$ in a LM |
| $R_0^2$ | $1 - \frac{SS_{RES}}{SS_{TOT}} = 1 - \frac{\sum_{i=1}^{n}(y_i - x_i)^2}{\sum_{i=1}^{n}(y_i)^2}$ (3) | Measure the variation in $y$ that is explained by $x$ in a one-to-one LM |

*Notation: $\sigma_{xy}$ is the covariance of x and y, $\sigma_x$ and $\sigma_y$ are standard deviations, n is the number of observations of $x$ and $y$, $y_i$ is $DMC_i$, $\bar{y}$ is the average of DCMs, and $x_i$ is the density layers related to DCM in each regression (e.g. DCM ~ BMLD). $SS_{RES}$ is the residual sum of squares, $SS_{TOT}$ is the total sum of squares.*

In the empirical LM, $R_{em}^2$ was calculated using the typical formula with the residual sum of squares ($SS_{RES}$) as the square of the difference of $y$ and $\hat{y}$ (estimated $y$ from the model) (Eq. 2)). In the one-to-one LM, the $SS_{RES}$ in $R_0^2$ was adapted by replacing $\hat{y}$ with $x$ (Eq. (3)), since the values of $x$ and $y$ are assumed to be equal in the one-to-one line regression and the difference between them should be zero. The two $R^2$ differ also for the denominator $SS_{TOT}$, which is the sum of squares about the average of the explanatory variable in $R_{em}^2$ and the sum of squares of the DCM values since in $R_0^2$ the value of DCM and DL equals.

Since the $SS_{TOT}$ adopted in the two formulae is different, the proportion of explained DCMs' variance by each DL can be compared only within each linear regression rather than across the one-to-one and empirical regressions. Therefore, the power of prediction among DLs was discussed within each type of LM.

## 3. Results

The presented algorithm identifying for MLD and BMLD was applied to 1273 profiles exhibiting a pycnocline. The associations of the density levels ($MLD_{0.01}$, $MLD_{0.02}$, MLD, $HPD_{0.01\text{-}BMLD}$, $HPD_{0.02\text{-}BMLD}$, $HPD_{MLD\text{-}BMLD}$, BMLD and Max $N^2$) with DCMs and the vertical distribution of Chl-a are described in Sect 3.1 and 3.2.

### 3.1 Vertical distribution of DCM and density levels

The depth of Chl-a maximum (DCM) was compared to eight different levels of the density profile that are summarized in surface mixed layer depth ($MLD_{0.01}$, $MLD_{0.02}$, MLD), below mixed layer depth (BMLD), the centre of the pycnocline ($HPD_{0.01\text{-}BMLD}$, $HPD_{0.02\text{-}BMLD}$, $HPD_{MLD\text{-}BMLD}$) and the depth of maximum buoyancy frequency squared (Max $N^2$) to evaluate i) the strength of a positive linear relationship between each DL and DCM, and ii) the prediction of DCM from each DL.

The observations carried out in the FoF and Tay region confirmed the subsurface presence of maxima Chl-a between April and August, with DCMs distributing on average (± standard deviation) at 19.29 ± 6.56 m. All the indicator classifying the surface mixed layer ($MLD_{0.01}$, $MLD_{0.02}$ and MLD) distributed generally shallower than DCMs (Fig. 4 a-c,

Table 3) with a rare coincidence of their vertical distribution (from 0.39% to 1.73% of the profiles, Table 3). In particular, the thresholds' methods used to identify MLD exhibited the lowest Spearman correlation amongst all DLs, having almost a zero correlation to DCMs ($\rho_S$ = -0.01 and 0.08 for $MLD_{0.01}$ and $MLD_{0.02}$, Table 3) and a limited contribution to define DCM's variability in empirical linear regressions ($R^2_{em}$ = 0.00 and 0.01, Table 3). The Major Axis analysis measured intercepts and slopes in $MLD_{0.01}$ and $MLD_{0.02}$ almost perpendicular to the $y$-axis due to the strong presence of DCMs in deep waters. Although a clear subsurface aggregation of Chl-a maxima occurs below the surface mixed layer (Fig. 4c), the MLD identified by the algorithm correlated better to DCM than $MLD_{0.01}$ and $MLD_{0.02}$, with a positive linear relationship between the two variables and a greater explained variance of DCM by the one-to-one and empirical linear regressions (Table 3). The coefficients measured by MA for MLD (Table 3) reported a positive correlation of DCMs, representing a gradual deepening of DCM with the top of the pycnocline.

Max $N^2$ is the density level performing least well after MLDs in predicting DCMs, although it showed the highest percentage of coincidence with DCMs (13.51% of the profiles, Table 3). Similar to MLDs, DCMs have been recorded in 64.96% of the profiles at layers deeper than Max $N^2$, indicating that Chl-a maxima area located in waters below surface mixing, at stratified regions within the pycnocline.

Overall, the centre of the pycnocline (HPDs) performed better than MLD and Max $N^2$, distributing closer to DCMs. $HPD_{MLD\text{-}BMLD}$ reported the highest correlation to DCMs ($\rho_S$ = 0.56), and the highest explained DCM's variance from the one-to-one ($R^2_0$ = 0.90) and empirical ($R^2_{em}$ = 0.31) linear regressions (Table 3). The location of DCMs is highly related to $HPD_{MLD\text{-}BMLD}$, although only 4.63% of the profiles presented DCMs and $HPD_{MLD\text{-}BMLD}$ at the same depth (Table 3). Many profiles exhibited DCM deeper than $HPD_{MLD\text{-}BMLD}$ (78.69%), of which 81.53% distributed DCMs above BMLD (hence, between $HPD_{MLD\text{-}BMLD}$ and BMLD). $HPD_{0.01\text{-}BMLD}$, $HPD_{0.02\text{-}BMLD}$ less related to DCMs in Spearman's correlation, MA, one-to-one and empirical linear regressions than the $HPD_{MLD\text{-}BMLD}$ (Table 3).

The below mixed layer depth, BMLD, exhibited a reverse condition compared to the other density levels by encompassing 78.32% of DCMs in waters above it (Table 3). BMLDs is the second variable after $HPD_{MLD\text{-}BMLD}$ with the highest correlation to DCMs ($\rho_S$ = 0.55). It is distributed at the same depth of DCMs in 7.86% of the profiles and linearly predicted the location of maxima Chl-a in both one-to-one and empirical linear regressions (Table 3). BMLD exhibited MA coefficients ($\alpha$ = 0.60 and $\beta$ = 0.82) close to the hypothesized one-to-one fitting-line ($\alpha$ = 0 and $\beta$ = 1), indicating a good approximation of DCMs at the base of the pycnocline. Moreover, DCMs distributed on average at 2.74 ± 5.21 m above BMLD, with a maximum distance above it equal to 22 m, and 27 m below it.

The overall distribution of DCMs is discernible mainly (> 95.84% of profiles) below the surface mixed layers (MLDs' indicators), within the deepest half of the pycnocline (between $HPD_{MLD\text{-}BMLD}$ and BMLD) and it is bounded for 78.32% of the observations above the BMLD. Although DCMs generally reflect the region with the highest concentration of Chl-a throughout the water column, the vertical distribution of Chl-a can vary in the proximity of DCMs and accumulate mainly above or below it. Hence, the ecological relevance of the density levels (DLs) has been investigated in comparison with the vertical distribution of Chl-a (Sect. 3.3).

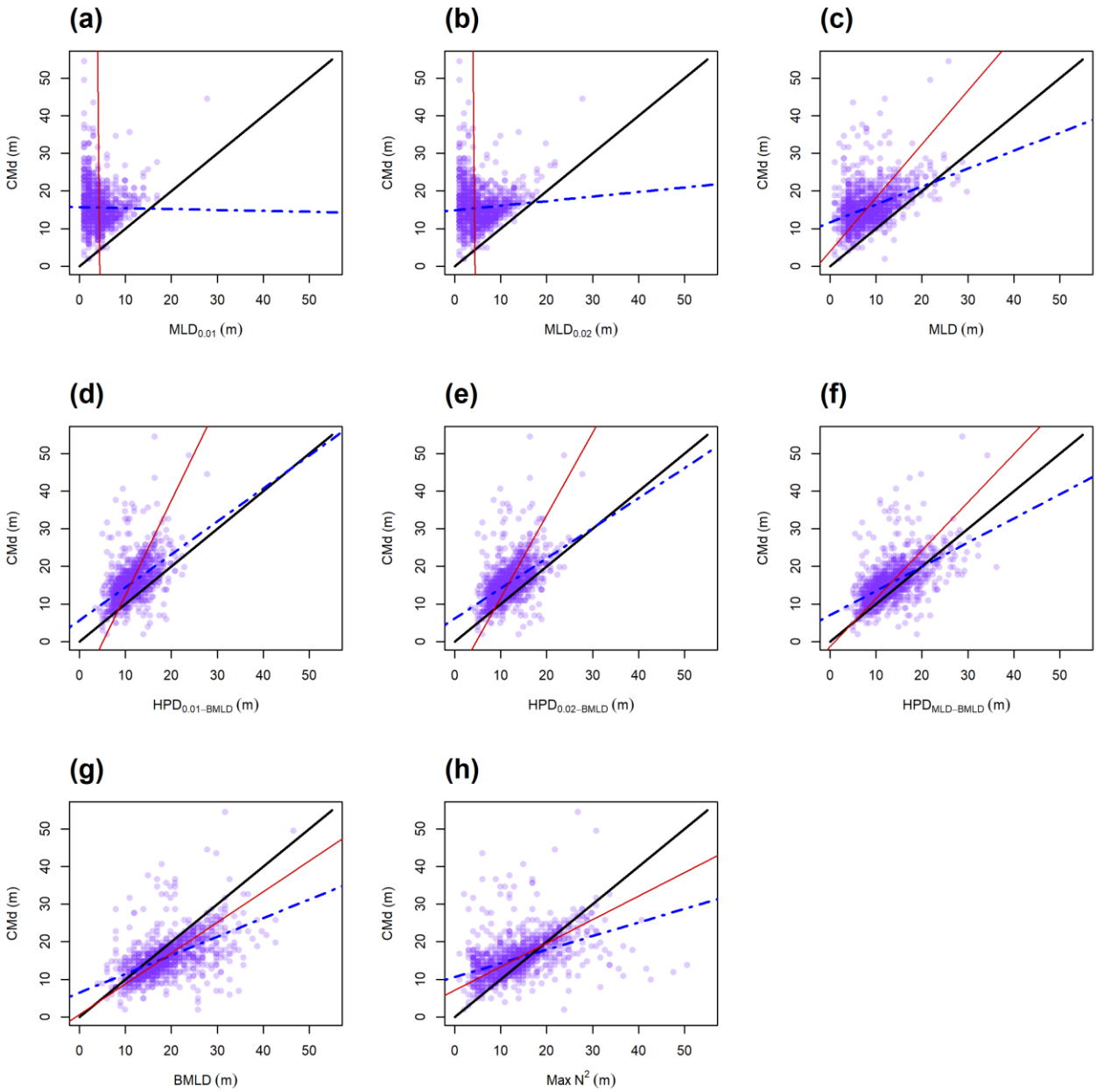


*Figure 4: Scatterplots of DCM and the eight DLs (a-h). The lines refer to the one-to-one linear regression (LM) (solid black), the Major Axis analysis (MA) (solid red), the empirical LM measured from the observations (DCM ~ DL) (dot-dashed blue). A good relationship between DL and DMC exhibits similar slope and intercept to the solid black line.*

*Table 3: Statistical parameters and percentage of profiles having DCMs above (>), at the same depth (=), or below (<) each DL. A good relationship is described by an $\alpha \sim 0$ and $\beta \sim 1$, high values of $\rho_S$, $R_0^2$, and $R_{em}^2$.*

| DL | $\rho_S$ | $\alpha$ | $\beta$ | $R_0^2$ | $R_{em}^2$ | DCM > DL | DCM = DL | DCM < DL |
|---|---|---|---|---|---|---|---|---|
| $MLD_{0.01}$ | - 0.01 | 543.35 | -124.26 | 0.40 | 0.00 | 99.53 | 0.39 | 0.08 |
| $MLD_{0.02}$ | 0.08 | -43.72 | 11.35 | 0.47 | 0.01 | 99.45 | 0.31 | 0.24 |
| MLD | 0.41 | 4.01 | 1.42 | 0.69 | 0.17 | 95.84 | 1.73 | 2.44 |
| $HPD_{0.01\text{-}BMLD}$ | 0.52 | -12.81 | 2.52 | 0.86 | 0.27 | 90.18 | 1.81 | 8.01 |
| $HPD_{0.02\text{-}BMLD}$ | 0.52 | -10.20 | 2.19 | 0.87 | 0.27 | 86.41 | 3.77 | 9.82 |
| $HPD_{MLD\text{-}BMLD}$ | 0.56 | 1.31 | 1.28 | 0.90 | 0.31 | 74.86 | 4.63 | 20.50 |
| BMLD | **0.55** | **0.60** | **0.82** | **0.87** | **0.31** | **13.83** | **7.86** | **78.32** |
| Max $N^2$ | 0.45 | 7.06 | 0.63 | 0.84 | 0.20 | 64.96 | 13.51 | 21.52 |

### 3.2 Chl-a vertical distribution in relation to density levels

Although DCMs generally reflect the region with the highest concentration of Chl-a throughout the water column, large concentration can still accumulate above or below it. Hydrodynamic and biological conditions generating resuspension, passive drift, and mortality (i.e. zooplankton grazing in stratified waters) can shape Chl-a differently throughout the water column, hence the ecological relevance of the density levels has been investigated in comparison with the vertical distribution of Chl-a.

The sum of depth-integrated Chl-a of all profiles was standardized by the number of observations (mg $m^{-3}$) above and below four DLs (MLD, $HPD_{MLD\text{-}BMLD}$, BMLD and Max $N^2$), in order to compare the overall Chl-a within each layer of the water column. MLD and $HPD_{MLD\text{-}BMLD}$ were selected amongst the density levels to represent the surface mixed layer and the centre of pycnoclines because of their better correlation to DCM (see Sect. 3.1). The total amount of Chl-a above and below the four density levels is reported as standardized depth-integrated values in Table 4 and shown at each meter depth in Figure 5.

Table 4: Sum of all depth-integrated Chl-a (mg $m^{-2}$) standardized by the number of observations above and below the four density layers.

| DL | Standardized depth-integrated (total) Chl-a above DL (mg $m^{-3}$) | Standardized depth-integrated (total) Chl-a below DL (mg $m^{-3}$) |
|---|---|---|
| MLD | 172.97 | 971.12 |
| $HPD_{MLD\text{-}BMLD}$ | 366.07 | 859.27 |
| BMLD | 615.92 | 658.72 |
| Max $N^2$ | 372.90 | 848.14 |

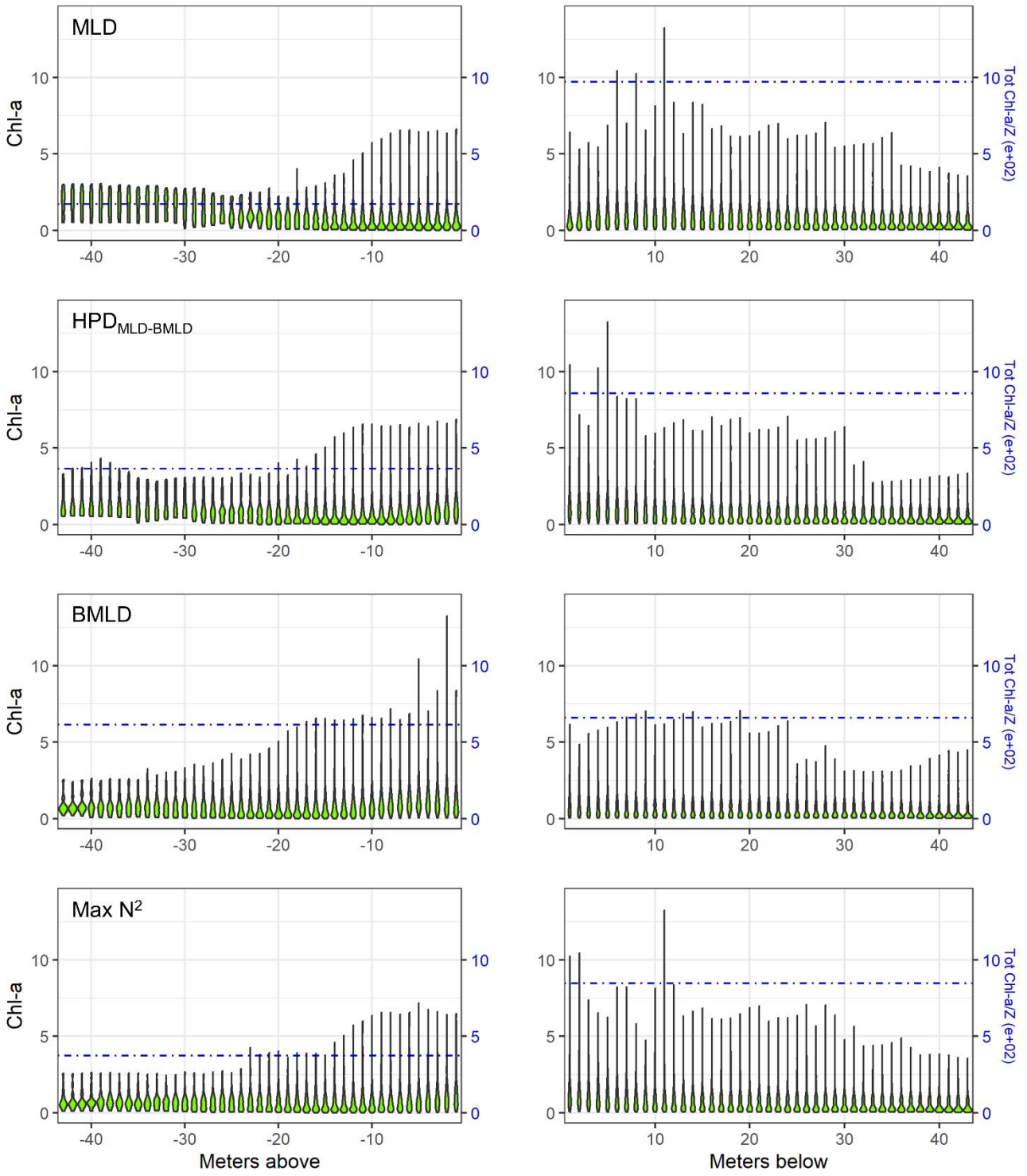


*Figure 5: Violin plot of Chl-a (mg) at each meter above and below the four density levels (MLD, $HPD_{MLD-BMLD}$, BMLD and Max $N^2$) for the whole dataset. The dot-dashed blue lines represent the standardized depth-integrated Chl-a measured as the total amount of Chl-a of all profiles (mg $m^{-2}$) divided by the number of depths (m) within each portion of the water column (above and below DLs).*

Following the results in Sect. 3.1, a large portion of Chl-a was measured at depths below MLD, $HPD_{MLD-BMLD}$ and Max $N^2$ (Table 4), where the depth of Chl-a maximum also occurred. From the seabed to $HPD_{MLD-BMLD}$ and Max $N^2$, the amount of Chl-a was three times the Chl-a from these DLs to the surface. A reverse condition occurred for Chl-a distributing above and below BMLDs: the standardized depth-integrated Chl-a is higher above BMLDs, although the amount of Chl-

a in the deepest layers (below the pycnocline) is still comparable (the difference between Chl-a from the surface to BMLD and from BMLD to seabed is 42.80 mg $m^{-1}$) (Table 4).

It is therefore sensible to infer the distribution of DCMs, and the largest portion of Chl-a, at depths enclosed within the stratified region (MLD – BMLD), especially in the second half of the pycnocline ($HPD_{MLD-BMLD}$ – BMLD). At the same time, a noticeable amount of Chl-a still distributes below the pycnocline (BMLD).

## 4. Discussion

In stratified waters, the vertical distribution of Chl-a is regulated by the balance of stratification and mixing rates across different hydrodynamic regimes over time (Leeuwen et al., 2015). The combination of static, dynamic and biological factors (e.g. grazing, Benoit-Bird *et al.*, 2013) induces phytoplankton communities to adapt their vertical distribution at small scales (< 1 km, Scott et al., 2010; Sharples et al., 2013). Identifying a proxy for subsurface concentrations of Chl-a is essential to investigate the impacts of physical changes due to large scale factors (e.g., stratification strength, sea level rise, or turbulence increase downstream wind turbine foundations). To date several studies have identified the mixed layer between the sea surface and the pycnocline as a valuable tool to assess changes in phytoplankton abundance and phenology over time; here we propose a tool to identify the vertical limits of the pycnocline and indicate the mixed layer depth below the pycnocline (BMLD) as a variable influencing the vertical distribution, abundance and phenology of Chl-a.

### 4.1 Ecological relevance of MLD and Max $N^2$ in defining DCMs

Oceanic sites often exhibited phytoplankton blooms within the upper mixed layer (e.g. Behrenfeld, 2010; Costa et al., 2020; Somavilla et al., 2017) to coincide with MLDs' vertical fluctuations due to e.g. windstorm events deepening the pycnocline into nutrient-enriched waters (Detoni et al., 2015; Carranza et al., 2018; Höfer et al., 2019; Montes-Hugo et al., 2009). Although MLD are linked to the physical processes setting the vertical distribution of DMCs in deep oceanic environments, all the investigated surface mixed layers' indicators ($MLD_{0.01}$, $MLD_{0.02}$ and MLD) weakly predicted DCM in the shelf waters investigated in this study. MLD has been largely considered as a central variable for understanding phytoplankton dynamics (Sverdrup, 1953), and its relation with climate change has been investigated to infer possible significant changes in the amount, spatial distribution and phenology of future primary production (Boyd et al., 2015; Montes-Hugo et al., 2009; Somavilla et al., 2017; Prend et al., 2019; Richardson and Bendtsen, 2019; Schmidt et al., 2020). The effects of climate change on MLD and primary production is still unclear (Lozier et al., 2011; Somavilla et al., 2017) and might be related to i) the large amount of Chl-a data required to investigate variations in primary production that have to rely on e.g. satellites' observations at the sea surface that leave out subsurface Chl-a (Baldry et al., 2020; Erickson et al., 2016; Lee et al., 2015), and ii) the exclusive investigation of the surface physics on primary production (e.g. temperature, wind-induced mixing) by neglecting deep processes that are responsible for the pycnocline's stability (Dave and Lozier, 2015, 2013; Lozier et al., 2011; Somavilla et al., 2017). The MLD is informative for surface concentrations, but it may not be biologically relevant for subsurface Chl-a that are maintained at the pycnocline by deep turbulent mixing. The need for a much more detailed understanding of the linkage between subsurface Chl-a, pycnocline characteristics and deep turbulent processes is therefore a key subject, especially in highly productive but spatially heterogeneous areas such as shelf waters and shallow seas.

In the FoF and Tay region, Max $N^2$ exhibited higher percentages of coincidence with DCMs (13.51% of 1273 profiles) than other DLs (Table 3). The depth of Max $N^2$ is a less turbulent region where the energy to exchange parcels in the vertical is maximum (Boehrer and Schultze, 2009), and it is frequently used to identify the upper mixed layer depth (e.g.

Carvalho et al., 2017). The location of DCMs at Max $N^2$ might reflect the distribution of phytoplankton within a less turbulent region where nutrient particles, which have been resuspended by mixing, can persist for longer time periods. The Max $N^2$ would therefore represent a mild turbulent layer where resuspended phytoplankton cells accumulate, while mixing processes above and/or below Max $N^2$ redistribute phytoplanktonic organisms throughout the water column. However, the amount of standardized depth-integrated Chl-a below Max $N^2$ is almost three times higher than above it (Table 4 and Fig. 5) suggesting that Max $N^2$ is a layer of suitable conditions for phytoplankton to grow, but it lacks informing where most of the Chl-a vertically distribute. Although the depth of Max $N^2$ appeared to better inform the exact location of DCMs, the percentage of its coincidence with DCMs is still low and might relate to specific conditions. Overall, the linear correlation ($\rho_S$), the MA coefficients and the one-to-one linear regression $R_0^2$ described a poor association of DCMs with Max $N^2$ compared to HPD indicators and BMLD, and hence the use of Max $N^2$ to locate subsurface Chl-a patches in summertime shelf waters may lead to underestimate the amount of Chl-a in the whole water column.

### 4.2 Vertical distribution of Chl-a and BMLD

The observations carried out in the FoF and Tay region confirmed the subsurface presence of maxima Chl-a between April and August. A recent study in the German Bight described DCMs located mainly at the centre of the pycnocline and the overall amount of Chl-a at depths distinctly lower than the surface mixed layers (Zhao et al., 2019a). The location of DCM at the pycnocline is regulated over time by upward nutrient-enriched fluxes entering the pycnocline from deep waters (Pingree et al., 1982; Rosenberg et al., 1990). In the Skagerrak strait between Denmark and Norway, deep SCM were recorded at a nutricline (rate of change in nitrate and phosphate) located below the base of a shallow pycnocline (< 15 m) (Bjørnsen et al., 1993). The low concentration of DCMs below BMLD might reflect a limited erosion of Chl-a by mixing (Zhao et al., 2019a) and, possibly, grazing (Benoit-Bird et al., 2013). The physical factors developing subsurface Chl-a are defined by mixing processes below the pycnocline that provides an indispensable upward flux of nutrients in the euphotic zone, where e.g. dinoflagellates are able to compete successfully in slightly turbulent conditions (< 0.1 mm $s^{-1}$) (Ross and Sharples, 2007). Therefore, the erosion as well as the resuspension of sinking phytoplankton cells and nutrients can maintain the proximity of DCMs at BMLDs setting the location of the nutricline at the base of the pycnocline. It is also noticeable that a large amount of diluted Chl-a in deep waters (51.67% of depth-integrated Chl-a below BMLD) might be crucial in maintaining primary production in the subsurface over the summer, since deep mixing processes eroding and sustaining Chl-a at BMLD would also contribute to reducing the overlap between SCM and predators (Behrenfeld, 2010). However, it should be noted that the high concentrations of Chl-a at DCM may reflect the photoacclimation of phytoplankton rather than an actual increase in carbon biomass (Marañón et al., 2021). Hence, the location of DCM close to the base of the pycnocline informs on a large concentration in pigments rather than in carbon production, which should be considered when DCM is used as a proxy of food patches. Overall, DCMs, and most of the depth-integrated Chl-a, distribute in the proximity of the centre and the base of the pycnocline suggesting the maintenance of subsurface Chl-a by deep turbulent fluxes which supply nutrients into the deepest portion of the pycnocline.

### 4.3 Using BMLD to investigate impacts on primary production

In this section are introduced some of the potential contexts in which BMLD's use would be advantageous. The linkage between the mixed layer depth below the pycnocline and subsurface Chl-a advocates BMLD as a key variable to address the effects of climate changes and man-made structures (e.g. offshore wind farm foundations) on the food resources, and defines BMLD as a potential proxy of subsurface food patches to investigate the vertical and spatial distribution of grazing and predator species.

*Climate change*

Since primary production is sustained by deep turbulent processes in prolonged stratified conditions, investigating the effect of future climate change, where stratification has been reported to increase over time (Capuzzo et al., 2018), using BMLD as a proxy of the vertical distribution of deep physical processes might be more informative than MLD in shelf waters. The Northeast Atlantic shelves experienced a summertime increase of stratification and a consequential reduction of Chl-a in the last 60 years in waters where nutrient fluxes had been confined in deep layers (Capuzzo et al., 2018; Schmidt et al., 2020). Prolonged stratified conditions are known to promote subsurface patches of Chl-a (Ross and Sharples 2007; Somavilla et al., 2017) due to the depletion of nutrients at shallow layers after surface blooms. The starvation of nutrients at the surface forces phytoplankton to re-distribute (e.g. Bindoff et al., 2019; Boyd et al., 2015; Schmidt et al., 2020) in deeper nutrient-enriched waters, within the euphotic zone. Hence, the location of DCMs in the proximity of the deepest portion of the pycnocline, between $HPD_{MLD\text{-}BMLD}$ and BMLD, (78.32% of the profiles) is not surprising during summer in the Firth of Forth and Tay regions, where the production of Chl-a is sustained by weak upward fluxes of nutrients from deep layers. The effects of an intensified stratification on primary production in the continental shelf waters are still entangled and suggest an overall deepening of subsurface Chl-a, which is likely to delineate a knock-on effect on redistributing most of the higher trophic levels (e.g., zooplankton, fish) and affect the foraging success of highly adapted species such as surface feeding seabirds (OSPAR, 2017). Hence, the role of climate change in increasing stratification is likely to affect the distribution of BMLD and the upward fluxes, which may either redistribute food patches and causing a variation in abundance and community composition of primary production (Holt et al., 2016, 2018; Capuzzo et al., 2018). The potential deepening of BMLD within or even below the euphotic zone may lead Chl-a to decrease across shelf seas since phytoplanktonic cells would increase buoyance at deeper and darker depths.

However, the deepening of productive patches is difficult to examine over large spatial scales, and remote sensing methods often lack reliability for subsurface data. The global estimates of carbon sequestration have often failed to include 10% to 40% of subsurface Chl-a (Sharples et al., 2001). Since the correct measurement of primary production throughout the whole water column is essential, key drivers of subsurface production are demanded to correctly predict, measure, and estimate DMCs from widely-used remote sensing data. Although data on the nutricline position were unavailable in this study, the vertical distribution of BMLD informed adequately on the position of subsurface productive patches in stratified waters, making this variable an important indicator of the vertical distribution of phytoplankton in shelf regions.

*Offshore renewable infrastructures*

It is reasonable to stress that potential effects on primary production involve both surface and deep (below the pycnocline) processes, especially where multiple local changes (i.e. wind turbine foundations changing levels of mixing) repeated over large spatial areas (i.e. the North Sea) can have an effect at different scales (van der Molen et al., 2014; De Dominicis et al., 2018; Carpenter et al., 2016). The upcoming interest of the offshore renewable sector in building offshore wind farms in stratified regions rises the need of drafting reliable environmental impact assessments able to identify key variables for estimating the effects in a holistic way (Dorrell et al., 2022). The consequences of offshore wind farms are likely to be related to bathymetry and mixing budgets, by affecting the stratification rate differently across depths. In this study area with spring tidal speeds < 1 $ms^{-1}$ , the vertical distribution of DCMs at BMLDs appeared to be correlated to the bathymetry by exhibiting DCMs closer to BMLDs at water depths comprised from, approximately, 40 to 70 m, DCMs deeper than BMLD mainly in shallow waters < 60 m, and DCMs above BMLD towards deeper waters up to 100 m (Fig. A3 in Appendix A). Previous studies identified a similar pattern in shallow waters (25-85 m) where DCMs were mainly recorded at or below the base of the pycnocline (Barth et al., 1998; Durán-Campos et al., 2019; Holligan et al., 1984;

Zhao et al., 2019a). Although stratification is reported to intensify in shelf waters with climate change, the increase in turbulence downstream of wind farms may counteract the local stratification (Carpenter et al., 2016; Schulien et al., 2017; Schultze et al., 2020) and affect the temporal and spatial distribution of Chl-a. Since the variation in stratification is a useful tool to address possible impacts on primary production, understanding the potential impacts on the vertical distribution of BMLD is likely to efficiently predict changes in the vertical distribution of Chl-a and its possible predators.

## 5. Conclusion

Chl-a vertical distribution provides important information about the state of development of the phytoplankton community which is associated with mixed and stratified layers. The mixing processes above and below the pycnocline can have very different influences on Chl-a vertical distribution, dictating the concentration at subsurface patches that can distribute close to, above, or below the pycnocline.

Although the association of phytoplankton with MLD has been largely described at large spatial scales within oceanic habitats, the presented study shows a weak linkage between MLD and DCM in shelf waters, at a very high vertical resolution (1 m). The results indicate that HPD indicators and BMLD, have a stronger association with summertime subsurface Chl-a maxima within the bottom-half of the pycnocline. Therefore deep mixing processes, such as tidal currents, play a role in regulating summertime subsurface primary production and regulate their distribution at BMLDs in the stratified conditions found in the North Sea. Considering the described associations of subsurface Chl-a with BMLD, it is evident how this variable can play a role in the assessment of productivity, since the deep mixing processes are equally (or more) relevant than the surface process in determining a shift of primary production at local and large scales. This association therefore advocates the investigation of the effect of anomaly-inducing processes occurring at and below the pycnocline (e.g. bottom temperature and salinity, turbulence and physical processes at the BMLD), which are likely to influence primary production and on to the whole ecosystem dynamics within shelf seas (Trifonova et al., 2021). Understanding mechanisms affecting primary production at fine scales is very important to investigate as we are moving rapidly towards the deployment of thousands of structures and hundreds of GW in wind energy extraction from worldwide shallow seas (Gielen et al., 2019). This work proposes BMLD as an ecological relevant variable for further oceanographic investigations in shelf waters, along with the proposed analytical approach as a valuable tool to extrapolate this variable from *in situ* vertical samples.

## Appendix A

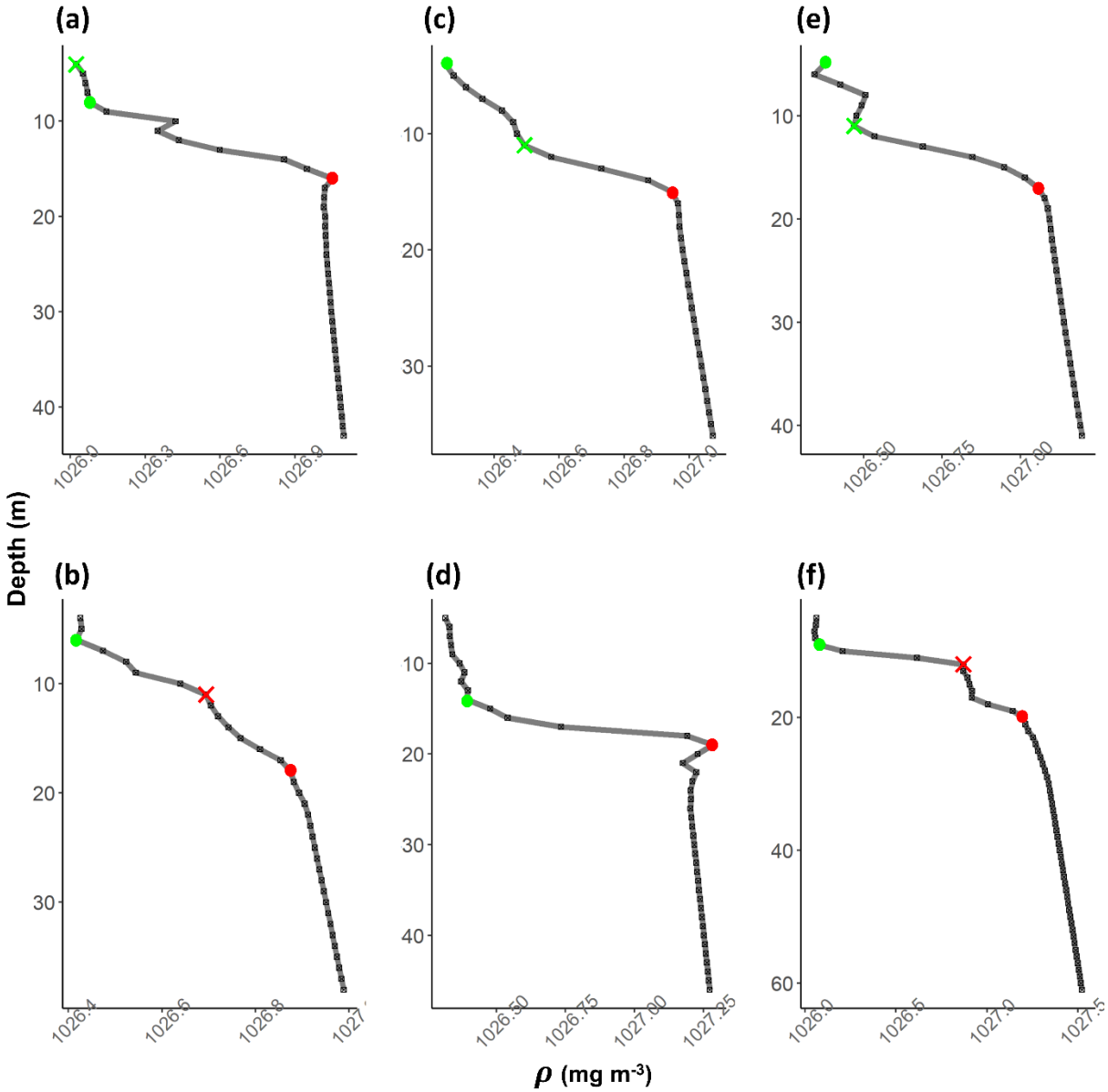


*Figure A1: examples of density profiles (grey line) (a-f). The black squares are observations at 1 m resolution. Red dots refer to BMLD, green dots to MLD. Crosses refer to misidentified MLD (in green) and BMLD (in red) that were manually corrected.*

535

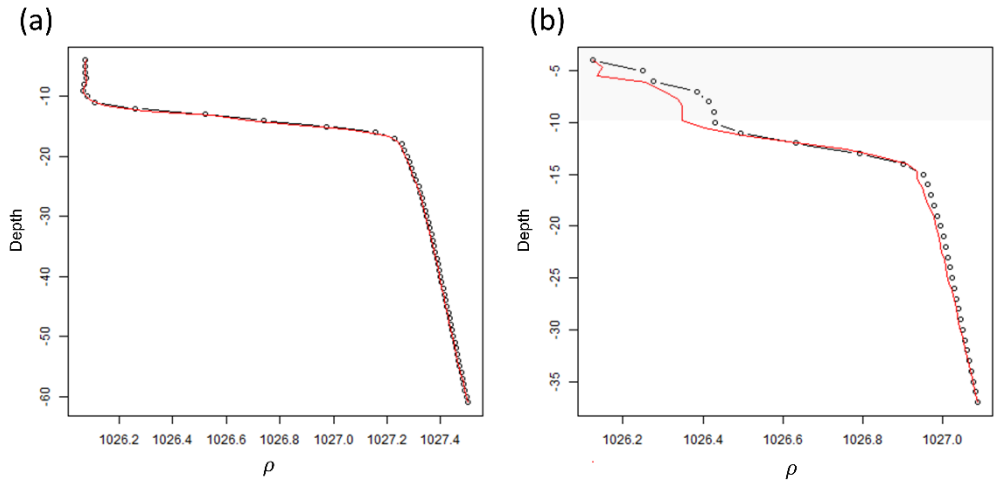


*Figure A2: two density profiles whose observations were standardized at equals 1 m intervals using generalized additive model (GAM). (a) density profile (black dotted line) where the GAM correctly fitted (red solid line) the vertical distribution. (b) density profile where the GAM wrongly fitted the upper portion of the profile (grey polygon area) and, hence, required a manual correction of the values.*

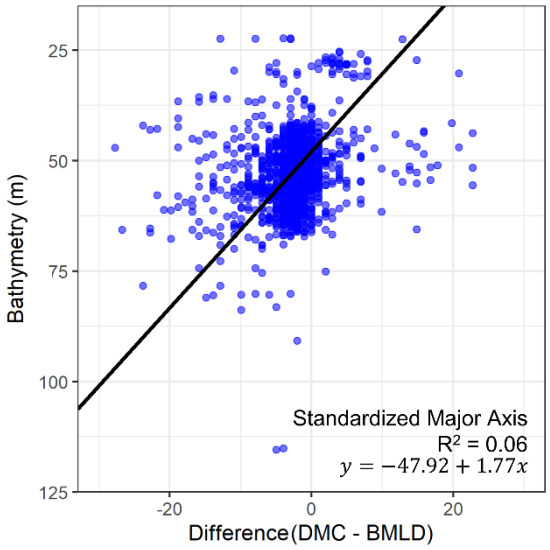


*Figure A3: scatterplot of the difference between DCM and BMLD against the bathymetry at which each profile was sampled. The solid black line reports a Standardized Major Axis analysis, whose equation and R squared values are reported.*

**Author contribution**

Arianna Zampollo contributed to the conceptualization of the study, formal analyses, methodology on MLD and BMLD, writing of the original draft, and software use; Thomas Cornulier contributed to the conceptualization and supervision of the statistical method, writing of the original draft, methodology and visualization of the results; Rory O'Hara Murray contributed on the data curation, writing of the original draft, supervision, visualization and validation;

Jacqueline F. Tweddle contributed to the conceptualization and the supervision of the study; James Dunning contributed to the methodology of the MLD and BMLD algorithm; Beth Scott contributed to the conceptualization of the analyses, writing of the original draft, revision of the two versions, contextualization and discussion of the results, supervision, funding acquisition, resources and data curation.

**Code availability**

The codes for the identification of DCM, MLD and BMLD are available at https://github.com/azampollo/BMLD

**Data availability**

Data are available upon request and agreement with the co-authors.

**Competing interests**

The authors declare that they have no conflict of interest.

**Acknowledgment**

The authors thank the founding MarCRF, the Marine Collaboration Research Forum jointly sponsored by the University of Aberdeen and Marine Scotland Science, and Marine Scotland Science to provide the CTD data.

**References**

Baetge, N., Graff, J. R., Behrenfeld, M. J., and Carlson, C. A.: Net Community Production, Dissolved Organic Carbon Accumulation, and Vertical Export in the Western North Atlantic, Front. Mar. Sci., 7, 227, https://doi.org/10.3389/fmars.2020.00227, 2020.

Baldry, K., Strutton, P. G., Hill, N. A., and Boyd, P. W.: Subsurface Chlorophyll-a Maxima in the Southern Ocean, Front. Mar. Sci., 7, 671, https://doi.org/10.3389/fmars.2020.00671, 2020.

Barth, J. A., Bogucki, D., Pierce, S. D., and Kosro, P. M.: Secondary circulation associated with a shelfbreak front, Geophys. Res. Lett., 25, 2761–2764, https://doi.org/10.1029/98GL02104, 1998.

Behrenfeld, M. J.: Abandoning Sverdrup's Critical Depth Hypothesis on phytoplankton blooms, Ecology, 91, 977–989, https://doi.org/10.1890/09-1207.1, 2010.

Benoit-Bird, K. J., Shroyer, E. L., and McManus, M. A.: A critical scale in plankton aggregations across coastal ecosystems: CRITICAL SCALE IN PLANKTON AGGREGATIONS, Geophys. Res. Lett., 40, 3968–3974, https://doi.org/10.1002/grl.50747, 2013.

Bindoff, N. L., Cheung, W. W. L., Kairo, J. G., Arístegui, J., Guinder, V. A., Hallberg, R., Hilmi, N., Jiao, N., O'Donoghue, S., Suga, T., Acar, S., Alava, J. J., Allison, E., Arbic, B., Bambridge, T., Boyd, P. W., Bruggeman, J., Butenschön, M., Chávez, F. P., Cheng, L., Cinar, M., Costa, D., Defeo, O., Djoundourian, S., Domingues, C., Eddy, T., Endres, S., Fox, A., Free, C., Frölicher, T., Gattuso, J.-P., Gerber, G., Hallegraef, G., Harrison, M., Hennige, S., Hindell, M., Hogg, A., Ito, T., Kenny, T.-A., Kroeker, K., Kwiatkowski, L., Lam, V. W. Y., Laüfkotter, C., LeBillon, P., Bris, N. L., Lotze, H., MacKinnon, J., de Marffy-Mantuano, A., Martel, P., Molinos, J. G., Moseman-Valtierra, S., Motau, A., Mulsow, S., Mutombo, K., Oyinlola, M., Poloczanska, E. S., Pascal, N., Philip, M., Purkey, S., Rathore, S., Rebelo, X., Reygondeau, G., Rice, J., Richardson, A., Riebesell, U., Roach, C., Rocklöv, J., Roberts, M., Sloyan, B., Smith, M., Shurety, A., Wabnitz, C., and Whalen, C.: Changing Ocean, Marine Ecosystems, and Dependent Communities, Mar. Ecosyst., 142, n.d.

Bjørnsen, P., Kaas, H., Kaas, H., Nielsen, T., Olesen, M., and Richardson, K.: Dynamics of a subsurface phytoplankton maximum in the Skagerrak, Mar. Ecol. Prog. Ser., 95, 279–294, https://doi.org/10.3354/meps095279, 1993.

Boehrer, B. and Schultze, M.: Density Stratification and Stability, in: Encyclopedia of Inland Waters, edited by: Likens, G. E., Academic Press, Oxford, 583–593, https://doi.org/10.1016/B978-012370626-3.00077-6, 2009.

Bonaduce, A., Staneva, J., Behrens, A., Bidlot, J.-R., and Wilcke, R. A. I.: Wave Climate Change in the North Sea and Baltic Sea, J. Mar. Sci. Eng., 7, 166, https://doi.org/10.3390/jmse7060166, 2019.

Boyd, P. W., Lennartz, S. T., Glover, D. M., and Doney, S. C.: Biological ramifications of climate-change-mediated oceanic multi-stressors, Nat. Clim. Change, 5, 71–79, https://doi.org/10.1038/nclimate2441, 2015.

Brown, Z. W., Lowry, K. E., Palmer, M. A., van Dijken, G. L., Mills, M. M., Pickart, R. S., and Arrigo, K. R.: Characterizing the subsurface chlorophyll a maximum in the Chukchi Sea and Canada Basin, Deep Sea Res. Part II Top. Stud. Oceanogr., 118, 88–104, https://doi.org/10.1016/j.dsr2.2015.02.010, 2015.

Capuzzo, E., Lynam, C. P., Barry, J., Stephens, D., Forster, R. M., Greenwood, N., McQuatters-Gollop, A., Silva, T., Leeuwen, S. M. van, and Engelhard, G. H.: A decline in primary production in the North Sea over 25 years, associated with reductions in zooplankton abundance and fish stock recruitment, Glob. Change Biol., 24, e352–e364, https://doi.org/10.1111/gcb.13916, 2018.

Carpenter, J. R., Merckelbach, L., Callies, U., Clark, S., Gaslikova, L., and Baschek, B.: Potential Impacts of Offshore Wind Farms on North Sea Stratification, PLOS ONE, 11, e0160830, https://doi.org/10.1371/journal.pone.0160830, 2016.

Carranza, M. M., Gille, S. T., Franks, P. J. S., Johnson, K. S., Pinkel, R., and Girton, J. B.: When Mixed Layers Are Not Mixed. Storm-Driven Mixing and Bio-optical Vertical Gradients in Mixed Layers of the Southern Ocean, J. Geophys. Res. Oceans, 123, 7264–7289, https://doi.org/10.1029/2018JC014416, 2018.

Carvalho, F., Kohut, J., Oliver, M. J., and Schofield, O.: Defining the ecologically relevant mixed-layer depth for Antarctica's coastal seas, Geophys. Res. Lett., 44, 338–345, https://doi.org/10.1002/2016GL071205, 2017.

Chiswell, S. M.: Annual cycles and spring blooms in phytoplankton: don't abandon Sverdrup completely, Mar. Ecol. Prog. Ser., 443, 39–50, https://doi.org/10.3354/meps09453, 2011.

Chu, P. C. and Fan, C.: Maximum angle method for determining mixed layer depth from seaglider data, J. Oceanogr., 67, 219–230, https://doi.org/10.1007/s10872-011-0019-2, 2011.

Chu, P. C. and Fan, C.: Global ocean synoptic thermocline gradient, isothermal-layer depth, and other upper ocean parameters, Sci. Data, 6, 119, https://doi.org/10.1038/s41597-019-0125-3, 2019.

Costa, R. R., Mendes, C. R. B., Tavano, V. M., Dotto, T. S., Kerr, R., Monteiro, T., Odebrecht, C., and Secchi, E. R.: Dynamics of an intense diatom bloom in the Northern Antarctic Peninsula, February 2016, Limnol. Oceanogr., 65, 2056–2075, https://doi.org/10.1002/lno.11437, 2020.

Courtois, P., Hu, X., Pennelly, C., Spence, P., and Myers, P. G.: Mixed layer depth calculation in deep convection regions in ocean numerical models, Ocean Model., 120, 60–78, https://doi.org/10.1016/j.ocemod.2017.10.007, 2017.

Cullen, J. J.: Subsurface Chlorophyll Maximum Layers: Enduring Enigma or Mystery Solved?, Annu. Rev. Mar. Sci., 7, 207–239, https://doi.org/10.1146/annurev-marine-010213-135111, 2015.

Dave, A. C. and Lozier, M. S.: Examining the global record of interannual variability in stratification and marine productivity in the low-latitude and mid-latitude ocean, J. Geophys. Res. Oceans, 118, 3114–3127, https://doi.org/10.1002/jgrc.20224, 2013.

Dave, A. C. and Lozier, M. S.: The impact of advection on stratification and chlorophyll variability in the equatorial Pacific, Geophys. Res. Lett., 42, 4523–4531, https://doi.org/10.1002/2015GL063290, 2015.

De Dominicis, M., Wolf, J., and O'Hara Murray, R.: Comparative Effects of Climate Change and Tidal Stream Energy Extraction in a Shelf Sea, J. Geophys. Res. Oceans, 123, 5041–5067, https://doi.org/10.1029/2018JC013832, 2018.

Detoni, A. M. S., de Souza, M. S., Garcia, C. A. E., Tavano, V. M., and Mata, M. M.: Environmental conditions during phytoplankton blooms in the vicinity of James Ross Island, east of the Antarctic Peninsula, Polar Biol., 38, 1111–1127, https://doi.org/10.1007/s00300-015-1670-7, 2015.

Diehl, S.: Phytoplankton, Light, and Nutrients in a Gradient of Mixing Depths: Theory, Ecology, 83, 386–398, https://doi.org/10.1890/0012-9658(2002)083[0386:PLANIA]2.0.CO;2, 2002.

Diehl, S., Berger, S., Ptacnik, R., and Wild, A.: Phytoplankton, Light, and Nutrients in a Gradient of Mixing Depths: Field Experiments, Ecology, 83, 399–411, https://doi.org/10.1890/0012-9658(2002)083[0399:PLANIA]2.0.CO;2, 2002.

Dorrell, R. M., Lloyd, C. J., Lincoln, B. J., Rippeth, T. P., Taylor, J. R., Caulfield, C. P., Sharples, J., Polton, J. A., Scannell, B. D., Greaves, D. M., Hall, R. A., and Simpson, J. H.: Anthropogenic Mixing in Seasonally Stratified Shelf Seas by Offshore Wind Farm Infrastructure, Front. Mar. Sci., 9, 2022.

D'Ortenzio, F., Lavigne, H., Besson, F., Claustre, H., Coppola, L., Garcia, N., Laës-Huon, A., Le Reste, S., Malardé, D., Migon, C., Morin, P., Mortier, L., Poteau, A., Prieur, L., Raimbault, P., and Testor, P.: Observing mixed layer depth, nitrate and chlorophyll concentrations in the northwestern Mediterranean: A combined satellite and $NO_3$ profiling floats experiment, Geophys. Res. Lett., 41, 6443–6451, https://doi.org/10.1002/2014GL061020, 2014.

Ducklow, H. W., Baker, K., Martinson, D. G., Quetin, L. B., Ross, R. M., Smith, R. C., Stammerjohn, S. E., Vernet, M., and Fraser, W.: Marine pelagic ecosystems: the West Antarctic Peninsula, Philos. Trans. R. Soc. B Biol. Sci., 362, 67–94, https://doi.org/10.1098/rstb.2006.1955, 2007.

Durán-Campos, E., Monreal-Gómez, M. A., Salas de León, D. A., and Coria-Monter, E.: Chlorophyll-a vertical distribution patterns during summer in the Bay of La Paz, Gulf of California, Mexico, Egypt. J. Aquat. Res., 45, 109–115, https://doi.org/10.1016/j.ejar.2019.04.003, 2019.

Erickson, Z. K., Thompson, A. F., Cassar, N., Sprintall, J., and Mazloff, M. R.: An advective mechanism for deep chlorophyll maxima formation in southern Drake Passage, Geophys. Res. Lett., 43, 10,846-10,855, https://doi.org/10.1002/2016GL070565, 2016.

Gielen, D., Gorini, R., Wagner, N., Leme, R., Gutierrez, L., Prakash, G., Asmelash, E., Janeiro, L., Gallina, G., Vale, G., Sani, L., Casals, X. G., Ferroukhi, R., Parajuli, B., Feng, J., Alexandri, E., Chewpreecha, U., Goldman, M., Heald, S., Stenning, J., Pollitt, H., García-Baños, C., and Renner, M.: Global energy Transformation: A Roadmap to 2050, 2019.

González-Pola, C., Fernández-Díaz, J. M., and Lavín, A.: Vertical structure of the upper ocean from profiles fitted to physically consistent functional forms, Deep Sea Res. Part Oceanogr. Res. Pap., 54, 1985–2004, https://doi.org/10.1016/j.dsr.2007.08.007, 2007.

Gradone, J. C., Oliver, M. J., Davies, A. R., Moffat, C., and Irwin, A.: Sea Surface Kinetic Energy as a Proxy for Phytoplankton Light Limitation in the Summer Pelagic Southern Ocean, J. Geophys. Res. Oceans, 125, e2019JC015646, https://doi.org/10.1029/2019JC015646, 2020.

Hickman, A., Moore, C., Sharples, J., Lucas, M., Tilstone, G., Krivtsov, V., and Holligan, P.: Primary production and nitrate uptake within the seasonal thermocline of a stratified shelf sea, Mar. Ecol. Prog. Ser., 463, 39–57, https://doi.org/10.3354/meps09836, 2012.

Höfer, J., Giesecke, R., Hopwood, M. J., Carrera, V., Alarcón, E., and González, H. E.: The role of water column stability and wind mixing in the production/export dynamics of two bays in the Western Antarctic Peninsula, Prog. Oceanogr., 174, 105–116, https://doi.org/10.1016/j.pocean.2019.01.005, 2019.

Holligan, P. M., Balch, W. M., and Yentsch, C. M.: The significance of subsurface chlorophyll, nitrite and ammonium maxima in relation to nitrogen for phytoplankton growth in stratified waters of the Gulf of Maine, J. Mar. Res., 42, 1051–1073, https://doi.org/10.1357/002224084788520747, 1984.

Holt, J., Schrum, C., Cannaby, H., Daewel, U., Allen, I., Artioli, Y., Bopp, L., Butenschon, M., Fach, B. A., Harle, J., Pushpadas, D., Salihoglu, B., and Wakelin, S.: Potential impacts of climate change on the primary production of regional seas: A comparative analysis of five European seas, Prog. Oceanogr., 140, 91–115, https://doi.org/10.1016/j.pocean.2015.11.004, 2016.

Holt, J., Polton, J., Huthnance, J., Wakelin, S., O'Dea, E., Harle, J., Yool, A., Artioli, Y., Blackford, J., Siddorn, J., and Inall, M.: Climate-Driven Change in the North Atlantic and Arctic Oceans Can Greatly Reduce the Circulation of the North Sea, Geophys. Res. Lett., 45, 11,827-11,836, https://doi.org/10.1029/2018GL078878, 2018.

Holte, J. and Talley, L.: A New Algorithm for Finding Mixed Layer Depths with Applications to Argo Data and Subantarctic Mode Water Formation, J. Atmospheric Ocean. Technol., 26, 1920–1939, https://doi.org/10.1175/2009JTECHO543.1, 2009.

Kara, A. B., Rochford, P. A., and Hurlburt, H. E.: An optimal definition for ocean mixed layer depth, J. Geophys. Res. Oceans, 105, 16803–16821, https://doi.org/10.1029/2000JC900072, 2000.

Klymak, J. M., Pinkel, R., and Rainville, L.: Direct Breaking of the Internal Tide near Topography: Kaena Ridge, Hawaii, J. Phys. Oceanogr., 38, 380–399, https://doi.org/10.1175/2007JPO3728.1, 2008.

Lee, Z., Marra, J., Perry, M. J., and Kahru, M.: Estimating oceanic primary productivity from ocean color remote sensing: A strategic assessment, J. Mar. Syst., 149, 50–59, https://doi.org/10.1016/j.jmarsys.2014.11.015, 2015.

Leeuwen, S. van, Tett, P., Mills, D., and Molen, J. van der: Stratified and nonstratified areas in the North Sea: Long-term variability and biological and policy implications, J. Geophys. Res. Oceans, 120, 4670–4686, https://doi.org/10.1002/2014JC010485, 2015.

Lips, U., Lips, I., Liblik, T., and Kuvaldina, N.: Processes responsible for the formation and maintenance of sub-surface chlorophyll maxima in the Gulf of Finland, Estuar. Coast. Shelf Sci., 88, 339–349, https://doi.org/10.1016/j.ecss.2010.04.015, 2010.

Lorbacher, K., Dommenget, D., Niiler, P. P., and Köhl, A.: Ocean mixed layer depth: A subsurface proxy of ocean-atmosphere variability, J. Geophys. Res. Oceans, 111, https://doi.org/10.1029/2003JC002157, 2006.

Lozier, M. S., Dave, A. C., Palter, J. B., Gerber, L. M., and Barber, R. T.: On the relationship between stratification and primary productivity in the North Atlantic, Geophys. Res. Lett., 38, https://doi.org/10.1029/2011GL049414, 2011.

Marañón, E., Van Wambeke, F., Uitz, J., Boss, E. S., Dimier, C., Dinasquet, J., Engel, A., Haëntjens, N., Pérez-Lorenzo, M., Taillandier, V., and Zäncker, B.: Deep maxima of phytoplankton biomass, primary production and bacterial production in the Mediterranean Sea, Biogeosciences, 18, 1749–1767, https://doi.org/10.5194/bg-18-1749-2021, 2021.

Martin, J., Tremblay, J.-É., Gagnon, J., Tremblay, G., Lapoussière, A., Jose, C., Poulin, M., Gosselin, M., Gratton, Y., and Michel, C.: Prevalence, structure and properties of subsurface chlorophyll maxima in Canadian Arctic waters, Mar. Ecol. Prog. Ser., 412, 69–84, https://doi.org/10.3354/meps08666, 2010.

van der Molen, J., Smith, H. C. M., Lepper, P., Limpenny, S., and Rees, J.: Predicting the large-scale consequences of offshore wind turbine array development on a North Sea ecosystem, Cont. Shelf Res., 85, 60–72, https://doi.org/10.1016/j.csr.2014.05.018, 2014.

Montégut, C. de B., Madec, G., Fischer, A. S., Lazar, A., and Iudicone, D.: Mixed layer depth over the global ocean: An examination of profile data and a profile-based climatology, J. Geophys. Res. Oceans, 109, https://doi.org/10.1029/2004JC002378, 2004.

Montes-Hugo, M., Doney, S. C., Ducklow, H. W., Fraser, W., Martinson, D., Stammerjohn, S. E., and Schofield, O.: Recent Changes in Phytoplankton Communities Associated with Rapid Regional Climate Change Along the Western Antarctic Peninsula, Science, 323, 1470–1473, https://doi.org/10.1126/science.1164533, 2009.

Müller, M., Cherniawsky, J. Y., Foreman, M. G. G., and von Storch, J.-S.: Seasonal variation of the M 2 tide, Ocean Dyn., 64, 159–177, https://doi.org/10.1007/s10236-013-0679-0, 2014.

Orihuela-Pinto, B., England, M. H., and Taschetto, A. S.: Interbasin and interhemispheric impacts of a collapsed Atlantic Overturning Circulation, Nat. Clim. Change, 12, 558–565, https://doi.org/10.1038/s41558-022-01380-y, 2022.

OSPAR Marine Bird Abundance: https://www.ospar.org/documents?v=7127, last access: 13 November 2017

Pingree, R. D., Holligan, P. M., Mardell, G. T., and Harris, R. P.: Vertical distribution of plankton in the skagerrak in relation to doming of the seasonal thermocline, Cont. Shelf Res., 1, 209–219, https://doi.org/10.1016/0278-4343(82)90005-X, 1982.

Prend, C. J., Gille, S. T., Talley, L. D., Mitchell, B. G., Rosso, I., and Mazloff, M. R.: Physical Drivers of Phytoplankton Bloom Initiation in the Southern Ocean's Scotia Sea, J. Geophys. Res. Oceans, 124, 5811–5826, https://doi.org/10.1029/2019JC015162, 2019.

Prézelin, B. B., Hofmann, E. E., Mengelt, C., and Klinck, J. M.: The linkage between Upper Circumpolar Deep Water (UCDW) and phytoplankton assemblages on the west Antarctic Peninsula continental shelf, J. Mar. Res., 58, 165–202, https://doi.org/10.1357/002224000321511133, 2000.

Prézelin, B. B., Hofmann, E. E., Moline, M., and Klinck, J. M.: Physical forcing of phytoplankton community structure and primary production in continental shelf waters of the Western Antarctic Peninsula, J. Mar. Res., 62, 419–460, https://doi.org/10.1357/0022240041446173, 2004.

Richardson, K. and Bendtsen, J.: Vertical distribution of phytoplankton and primary production in relation to nutricline depth in the open ocean, Mar. Ecol. Prog. Ser., 620, 33–46, https://doi.org/10.3354/meps12960, 2019.

Richardson, K. and Pedersen, F. B.: Estimation of new production in the North Sea: consequences for temporal and spatial variability of phytoplankton, ICES J. Mar. Sci., 55, 574–580, https://doi.org/10.1006/jmsc.1998.0402, 1998.

Rosenberg, R., Dahl, E., Edler, L., Fyrberg, L., Granéli, E., Granéli, W., Hagström, Å., Lindahl, O., Matos, M. O., Pettersson, K., Sahlsten, E., Tiselius, P., Turk, V., and Wikner, J.: Pelagic nutrient and energy transfer during spring in the open and coastal Skagerrak, Mar. Ecol. Prog. Ser., 61, 215–231, 1990.

Ross, O. N. and Sharples, J.: Phytoplankton motility and the competition for nutrients in the thermocline, Mar. Ecol. Prog. Ser., 347, 21–38, https://doi.org/10.3354/meps06999, 2007.

Ryan-Keogh, T. J. and Thomalla, S. J.: Deriving a Proxy for Iron Limitation From Chlorophyll Fluorescence on Buoyancy Gliders, Front. Mar. Sci., 7, 275, https://doi.org/10.3389/fmars.2020.00275, 2020.

Schmidt, K., Birchill, A. J., Atkinson, A., Brewin, R. J. W., Clark, J. R., Hickman, A. E., Johns, D. G., Lohan, M. C., Milne, A., Pardo, S., Polimene, L., Smyth, T. J., Tarran, G. A., Widdicombe, C. E., Woodward, E. M. S., and Ussher, S. J.: Increasing picocyanobacteria success in shelf waters contributes to long-term food web degradation, Glob. Change Biol., https://doi.org/10.1111/gcb.15161, 2020.

Schofield, O., Miles, T., Alderkamp, A.-C., Lee, S., Haskins, C., Rogalsky, E., Sipler, R., Sherrell, R. M., and Yager, P. L.: *In situ* phytoplankton distributions in the Amundsen Sea Polynya measured by autonomous gliders, Elem. Sci. Anthr., 3, 000073, https://doi.org/10.12952/journal.elementa.000073, 2015.

Schulien, J. A., Behrenfeld, M. J., Hair, J. W., Hostetler, C. A., and Twardowski, M. S.: Vertically- resolved phytoplankton carbon and net primary production from a high spectral resolution lidar, Opt. Express, 25, 13577, https://doi.org/10.1364/OE.25.013577, 2017.

Schultze, L. K. P., Merckelbach, L. M., Horstmann, J., Raasch, S., and Carpenter, J. R.: Increased Mixing and Turbulence in the Wake of Offshore Wind Farm Foundations, J. Geophys. Res. Oceans, 125, e2019JC015858, https://doi.org/10.1029/2019JC015858, 2020.

Scott, B. E., Sharples, J., Ross, O. N., Wang, J., Pierce, G. J., and Camphuysen, C. J.: Sub-surface hotspots in shallow seas: fine-scale limited locations of top predator foraging habitat indicated by tidal mixing and sub-surface chlorophyll, Mar. Ecol. Prog. Ser., 408, 207–226, https://doi.org/10.3354/meps08552, 2010.

Sharples, J., Moore, M. C., Rippeth, T. P., Holligan, P. M., Hydes, D. J., Fisher, N. R., and Simpson, J. H.: Phytoplankton distribution and survival in the thermocline, Limnol. Oceanogr., 46, 486–496, https://doi.org/10.4319/lo.2001.46.3.0486, 2001.

Sharples, J., Ross, O. N., Scott, B. E., Greenstreet, S. P. R., and Fraser, H.: Inter-annual variability in the timing of stratification and the spring bloom in the North-western North Sea, Cont. Shelf Res., 26, 733–751, https://doi.org/10.1016/j.csr.2006.01.011, 2006.

Sharples, J., Scott, B. E., and Inall, M. E.: From physics to fishing over a shelf sea bank, Prog. Oceanogr., 117, 1–8, https://doi.org/10.1016/j.pocean.2013.06.015, 2013.

Somavilla, R., González-Pola, C., and Fernández-Diaz, J.: The warmer the ocean surface, the shallower the mixed layer. How much of this is true?, J. Geophys. Res. Oceans, 122, 7698–7716, https://doi.org/10.1002/2017JC013125, 2017.

Steinacher, M., Joos, F., Frölicher, T. L., Bopp, L., Cadule, P., Cocco, V., Doney, S. C., Gehlen, M., Lindsay, K., Moore, J. K., Schneider, B., and Segschneider, J.: Projected 21st century decrease in marine productivity: a multi-model analysis, Biogeosciences, 7, 979–1005, https://doi.org/10.5194/bg-7-979-2010, 2010.

Taboada, F. G. and Anadón, R.: Patterns of change in sea surface temperature in the North Atlantic during the last three decades: beyond mean trends, Clim. Change, 115, 419–431, https://doi.org/10.1007/s10584-012-0485-6, 2012.

Takahashi, M. and Hori, T.: Abundance of picophytoplankton in the subsurface chlorophyll maximum layer in subtropical and tropical waters, Mar. Biol., 79, 177–186, https://doi.org/10.1007/BF00951826, 1984.

Thomson, R. E. and Fine, I. V.: Estimating Mixed Layer Depth from Oceanic Profile Data, J. Atmospheric Ocean. Technol., 20, 319–329, https://doi.org/10.1175/1520-0426(2003)020<0319:EMLDFO>2.0.CO;2, 2003.

Trifonova, N. I., Scott, B. E., De Dominicis, M., Waggitt, J. J., and Wolf, J.: Bayesian network modelling provides spatial and temporal understanding of ecosystem dynamics within shallow shelf seas, Ecol. Indic., 129, 107997, https://doi.org/10.1016/j.ecolind.2021.107997, 2021.

Walsby, A. E.: Numerical integration of phytoplankton photosynthesis through time and depth in a water column, New Phytol., 136, 189–209, https://doi.org/10.1046/j.1469-8137.1997.00736.x, 1997.

Warton, D. I., Wright, I. J., Falster, D. S., and Westoby, M.: Bivariate line-fitting methods for allometry, Biol. Rev., 81, 259–291, https://doi.org/10.1017/S1464793106007007, 2006.

Weston, K., Fernand, L., Mills, D. K., Delahunty, R., and Brown, J.: Primary production in the deep chlorophyll maximum of the central North Sea, J. Plankton Res., 27, 909–922, https://doi.org/10.1093/plankt/fbi064, 2005.

Yentsch, C. S.: Influence of geostrophy on primary production. [Effect of ocean currents on nutrients of ocean water], Tethys Fr., 6:1–2, 1974.

Yentsch, C. S.: Phytoplankton Growth in the Sea, in: Primary Productivity in the Sea, edited by: Falkowski, P. G., Springer US, Boston, MA, 17–32, https://doi.org/10.1007/978-1-4684-3890-1_2, 1980.

Zhang, W.-Z., Wang, H., Chai, F., and Qiu, G.: Physical drivers of chlorophyll variability in the open South China Sea, J. Geophys. Res. Oceans, 121, 7123–7140, https://doi.org/10.1002/2016JC011983, 2016.

Zhao, C., Maerz, J., Hofmeister, R., Röttgers, R., Wirtz, K., Riethmüller, R., and Schrum, C.: Characterizing the vertical distribution of chlorophyll a in the German Bight, Cont. Shelf Res., 175, 127–146, https://doi.org/10.1016/j.csr.2019.01.012, 2019a.

Zhao, C., Daewel, U., and Schrum, C.: Tidal impacts on primary production in the North Sea, Earth Syst. Dyn., 10, 287–317, https://doi.org/10.5194/esd-10-287-2019, 2019b.